The Astrophysical Journal Letters, 889:L15 (5pp), 2020 January 20 https://doi.org/10.3847/2041-8213/ab6a14

Constraints on Aquatic Photosynthesis for Terrestrial Planets around Other Stars

Manasvi Lingam[1,2] and Abraham Loeb[2]
[1] Department of Aerospace, Physics and Space Sciences, Florida Institute of Technology, Melbourne, FL 32901, USA; mlingam@fit.edu
[2] Institute for Theory and Computation, Harvard University, Cambridge, MA 02138, USA
Received 2019 December 9; revised 2020 January 9; accepted 2020 January 10; published 2020 January 22

Abstract

Aquatic photosynthesis plays a major role in carbon fixation and O_2 production on Earth. In this Letter, we analyze the prospects for oxygenic photosynthesis in aquatic environments on modern Earth-analogs around F-, G-, K-, and M-type stars. Our analysis takes into account the spectral type of the host star, attenuation of light by aquatic organisms, and rates of respiration and photosynthesis. We study the compensation depth ($\mathcal{Z}_{\rm CO}$) and the critical depth ($\mathcal{Z}_{\rm CR}$), defined respectively as the locations where the net growth rates and vertically integrated net growth rates of photoautotrophs become zero. Our analysis suggests that $\mathcal{Z}_{\rm CO}$ declines by more than an order of magnitude as one moves from the habitable zones around Sun-like stars to late-type M-dwarfs, but $\mathcal{Z}_{\rm CR}$ decreases by only a modest amount (∼40%). For M-dwarf exoplanets, we propose that the photosynthetic red edge may constitute a more robust biosignature of aquatic photosynthesis compared to atmospheric O_2.

Unified Astronomy Thesaurus concepts: Astrobiology (74); Extrasolar rocky planets (511); Habitable planets (695); Exoplanet surface characteristics (496); Exoplanet surface composition (2022); Biosignatures (2018)

1. Introduction

The overwhelming majority of carbon fixation and biomass on Earth occurs via oxygenic photosynthesis (Knoll 2015). One of the chief reasons behind the proliferation of oxygenic photosynthesis on Earth is that the electron donor (water) was not limited in terms of availability, unlike other variants of photosynthesis (Ward et al. 2019). The wavelength range for oxygenic photosynthesis on Earth is approximately 350–750 nm (Chen & Blankenship 2011; Nürnberg et al. 2018), but most of the light utilized by oxygenic photoautotrophs lies within $\lambda_{\rm min} = 400$ nm and $\lambda_{\rm max} = 700$ nm, due to which it has been termed photosynthetically active radiation or PAR for short (Blankenship 2014, Chapter 1.2).[3]

Oceans are known to contribute around 50% of the total primary production on Earth (Field et al. 1998). A substantial fraction of terrestrial exoplanets, colloquially referred to as ocean planets, are expected to possess high water inventories, thereby hosting deep oceans and no continents at their surfaces (Tian & Ida 2015; Zain et al. 2018). Some of the planets of the well-known TRAPPIST-1 system, for instance, seemingly fall in this category (Grimm et al. 2018; Unterborn et al. 2018). It is therefore essential for studies of planetary habitability to analyze the prospects for aquatic photosynthesis.

However, this field has witnessed comparatively few analyses despite its importance. Wolstencroft & Raven (2002) modeled the global rates of O_2 production by Earth-like photoautotrophs at a fixed depth of 10 m underwater for stars of different spectral types. Kiang et al. (2007) estimated the PAR fluxes at depths of 0.05 m and 1 m for various stars, and analyzed the maximum wavelengths at which photosynthesis could operate. However, in order to properly gauge the maximal depths where photoautotrophs may occur, it is necessary to account for biological functions such as respiration and photosynthesis rates. A recent analysis along these lines was undertaken by Ritchie et al. (2018), but in the specific context of Proxima b. A similar study, ostensibly for the euphotic zone depth, for cool stars is briefly outlined in Kaltenegger (2019).

In this Letter, we will examine under what conditions aquatic photosynthesis is feasible and how its essential features are sensitive to the choice of host star. We will incorporate hitherto neglected effects and concepts (e.g., critical depth) and tackle modern Earth-analogs orbiting F-, G-, K-, and M-type stars.

2. Characteristics of Aquatic Photosynthesis

We will explore how stellar properties regulate key aspects of aquatic photosynthesis for rocky planets situated in the habitable zones (HZs) of their host stars (Kasting et al. 1993).

2.1. Mathematical Preliminaries

A rigorous assessment of aquatic photosynthesis requires an in-depth knowledge of biological (e.g., phytoplankton respiration and photosynthesis rates), geological (atmospheric and oceanic composition), and astrophysical (e.g., stellar temperature and flux) parameters. Owing to this complexity, we will hold all factors aside from the stellar properties fixed. The hypothetical planet in question is thus assumed to possess geological and biological attributes akin to Earth.

The flux incident at the top of Earth's atmosphere is $S_\oplus \approx 1360\ {\rm W\ m^{-2}}$, and we will suppose that the planet also receives the same amount of stellar flux. Furthermore, for the sake of simplicity, the planet is assumed to be optically thin across the PAR range analogous to modern Earth (Jacob 1999). Thus, we ignore attenuation of PAR during its passage through the atmosphere. When the star is at the substellar point, the photon flux density at that specific location on the planetary surface (denoted by $\mathcal{N}_{\rm max}$) is estimated as

$$\mathcal{N}_{\rm max}(\lambda) \approx n_\lambda \left(\frac{R_\star}{d_\star}\right)^2, \tag{1}$$

where $R_\star$ is the stellar radius and $d_\star$ is the orbital radius of the Earth-analog, while n_λ represents the photon flux density of the

[3] The upper wavelength of PAR may extend beyond 1000 nm in principle, but this would entail "exotic" multi-photon schemes (Wolstencroft & Raven 2002; Kiang et al. 2007; Lingam & Loeb 2019a) that lie beyond the scope of this work.

star. When the latter is modeled as a blackbody with an effective stellar temperature of T, the photon flux density becomes

$$n_\lambda = \frac{B_\lambda}{(hc/\lambda)} = \frac{2c}{\lambda^4}\left[\exp\left(\frac{hc}{\lambda k_B T}\right) - 1\right]^{-1}, \tag{2}$$

where B_λ is the spectral radiance given by the Planck function. We can express $d_\star$ in terms of the stellar properties by invoking the constraint

$$S_\oplus = \frac{L_\star}{4\pi d_\star^2} = \text{const}, \tag{3}$$

with the stellar luminosity defined as $L_\star = 4\pi\sigma R_\star^2 T^4$. Thus, upon substituting this result in (1), we arrive at

$$\mathcal{N}_{\max}(\lambda) \approx \frac{n_\lambda S_\oplus}{\sigma T^4}, \tag{4}$$

with the dependence on $R_\star$ being eliminated. However, we note that $\mathcal{N}_{\max}$ represents the maximum photon flux density because it ignores the effects of clouds and is calculated at the zenith, thus ignoring the rotation of the planet. A more realistic measure of the photon flux density ($\mathcal{N}_{\text{avg}}$), constituting its temporal average, is

$$\mathcal{N}_{\text{avg}}(\lambda) \approx \mathcal{N}_{\max}(\lambda) \cdot f_{\text{I}} \cdot f_{\text{CL}}, \tag{5}$$

where f_{I} accounts for the variation in the intensity of light at a given location, and f_{CL} embodies the additional attenuation introduced by clouds (Sarmiento & Gruber 2006, Chapter 4.2). For planets that are not tidally locked, $f_{\text{I}} \approx 1/4$ because the stellar radiation is intercepted across a cross-sectional area of πR^2 (where R is the planetary radius) but is subsequently distributed over the total surface area of $4\pi R^2$.[4] However, for tidally locked exoplanets, the radiation must be evenly distributed over the surface area of $2\pi R^2$ because of the permanently dark nightside, which yields $f_{\text{I}} \approx 1/2$. Determining the stellar "cutoff" at which Earth-analogs become tidally locked is difficult because the tidal locking timescale depends on numerous factors such as initial spin period, tidal dissipation factor, and presence/absence of moons (Barnes 2017).

Next, we turn our attention to the cloud fraction. General circulation models suggest that tidally locked planets at the inner edge of the HZ may manifest relatively high cloud coverage on their dayside; the resulting planetary albedo could become twice that of Earth (Yang et al. 2013, Section 3). Thus, on the one hand, f_{I} is elevated for tidally locked exoplanets. On the other, f_{CL} is potentially lower due to the greater attenuation from clouds. Hence, we will hold $f_A \equiv f_{\text{I}} \cdot f_{\text{CL}}$ fixed as our ensuing results will exhibit a logarithmic dependence on this parameter. We specify $f_A \approx 0.2$ to preserve consistency with Earth's parameters (Sarmiento & Gruber 2006, Chapter 4.3), which transforms (5) into $\mathcal{N}_{\text{avg}}(\lambda) \approx 0.2\mathcal{N}_{\max}(\lambda)$.

[4] The same result is obtained if the intensity is modeled as a triangular function of time (Sarmiento & Gruber 2006, Chapter 4.2).

The photon flux $\mathcal{F}$ at a depth z below the surface can be determined by employing

$$\mathcal{F}(z) \approx \int_{\lambda_{\min}}^{\lambda_{\max}} \mathcal{N}_0(\lambda)\exp\left[-K(\lambda)z\right] d\lambda, \tag{6}$$

where $\mathcal{N}_0(\lambda)$ is the photon flux density at the surface and is set by either $\mathcal{N}_{\max}$ or $\mathcal{N}_{\text{avg}}$ depending on the context. In the above formula, $K(\lambda)$ represents the vertical attenuation coefficient that is further decomposed into $K = K_W + K_C + K_B$, where K_W, K_C, and K_B denote the partial attenuation coefficients arising from clear water, chemical (both organic and inorganic) compounds, and biota, respectively (Kirk 2011, Chapter 9.5). In actuality, K_W, K_C, and K_B are complex functions of the wavelength and depth, thereby rendering subsequent calculations difficult to undertake.

We will therefore restrict our scope to encompass two distinct cases henceforth. In both instances, to simplify matters, we set $K_C \to 0$ and adopt

$$K_W(\lambda) \approx 1.4 \times 10^{-5}\,\text{m}^{-1}\exp\left(\lambda \cdot 1.54 \times 10^{7}\,\text{m}^{-1}\right) \tag{7}$$

across the PAR range because $K_W(\lambda)$ is well approximated by an exponential function; the corresponding data were taken from Pope & Fry (1997, Table 3). In the first, we select $\mathcal{N}_0(\lambda) = \mathcal{N}_{\max}$ and $K_B \to 0$, which constitutes the most optimal scenario wherein the star is at the zenith and no biological attenuation in present. In the second, we utilize $\mathcal{N}_0(\lambda) = \mathcal{N}_{\text{avg}}$ and $K_B \approx 0.08\ \text{m}^{-1}$ (Sarmiento & Gruber 2006, Chapter 4.2). This setup is more realistic because the dual affects of temporally averaged stellar flux and biological attenuation in water are incorporated. The two cases will be henceforth be identified by the use of the "M" (i.e., maximal) and "R" (i.e., realistic) superscripts.

Although we draw upon the salient characteristics of phytoplankton, this does not imply that the same organisms would necessarily evolve on other worlds; instead, it is merely assumed that their functional attributes are similar. The chief rationale behind employing eukaryotic phytoplankton as a proxy for putative aquatic biota is that they constitute the dominant source of carbon fixation in Earth's present-day oceans (Field et al. 1998; Raven 2009), and comprise the bedrock of current aquatic ecosystems (Valiela 2015). It is, therefore, worth exploring how a modern Earth-like aquatic biosphere would fare on Earth-analogs around other stars.

At this stage, a comment regarding the euphotic zone is in order. This zone is typically defined as the depth ($\mathcal{Z}_{\text{E}}$) at which the intensity is 1% of its surface value (Kirk 2011, Chapter 6.3). For an Earth-analog around a Sun-like star, most of the radiation that penetrates to a depth greater than few meters lies within the PAR range. Hence, utilizing the prior expressions for K yields $\mathcal{Z}_{\text{E}}^{(M)} \approx 277$ m and $\mathcal{Z}_{\text{E}}^{(R)} \approx 37$ m. The latter exhibits good agreement with the empirically derived range of 4.3–82.0 m (Lee et al. 2007) and the theoretical mean value of 38 m estimated in Sarmiento & Gruber (2006, Chapter 4.2) for $\mathcal{Z}_{\text{E}}$. In contrast, for an Earth-analog orbiting a late-type M-dwarf, most of the incident radiation falls within the near-infrared (near-IR), thereby yielding $K \gtrsim 1\ \text{m}^{-1}$ (Kou et al. 1993). As per the above definition, we obtain $\mathcal{Z}_{\text{E}} \lesssim 5$ m, which is consistent with analyses by Ritchie et al. (2018) and Kaltenegger (2019).

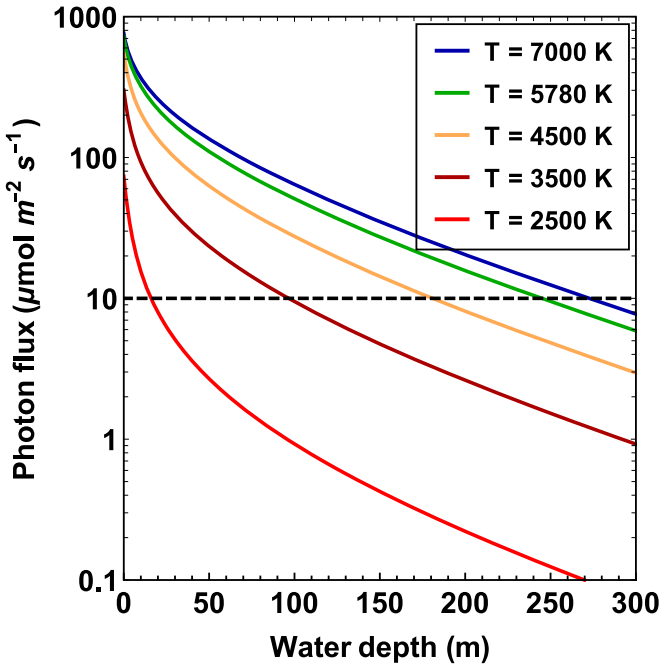

Figure 1. The maximal photon flux (in μmol m^{-2} s^{-1}) is shown as a function of the depth for Earth-analogs around FGKM stars; the curves correspond to different stellar temperatures. The horizontal dashed line yields the compensation depth, where the rates of photosynthesis and respiration balance each other.

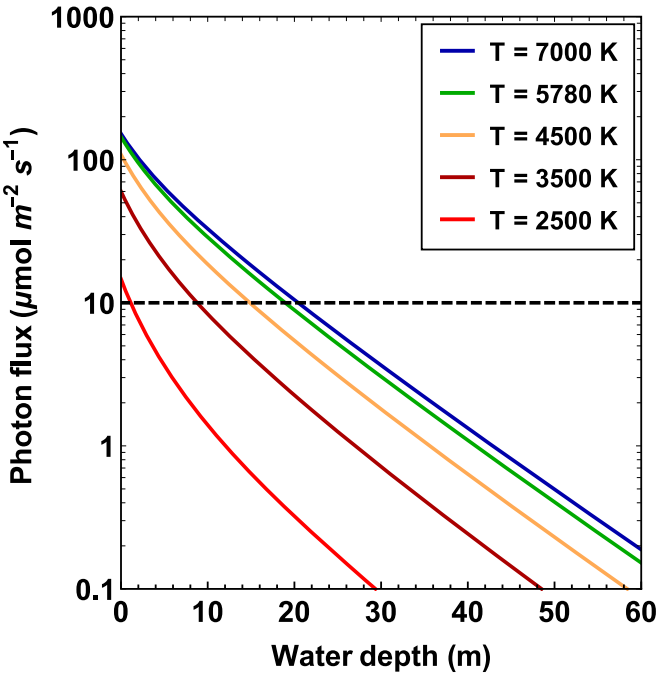

Figure 2. The photon flux (in μmol m^{-2} s^{-1}) is shown as a function of the depth for Earth-analogs around FGKM stars; the curves correspond to different stellar temperatures. The horizontal dashed line yields the compensation depth, where the rates of photosynthesis and respiration balance each other. In this model, time-averaged photon flux and aquatic biological attenuation are incorporated.

2.2. Critical Depth and Compensation Depth

Although the euphotic zone depth has some intrinsic value, it does not yield information concerning the maximal depths where photoautotrophs can exist. In order to estimate these quantities, we will analyze the *compensation* and *critical* depths, both of which were elucidated in the seminal work by Sverdrup (1953).

The compensation depth ($\mathcal{Z}_{\rm CO}$) is defined at the location where the rate of photosynthesis is sufficient to balance the respiration rate. At greater depths, respiration will dominate over photosynthesis, thus inhibiting the growth of the photosynthetic community. The photon flux at which this critical balance occurs is the compensation flux ($\mathcal{F}_C$). By supposing that the oxygenic photoautotrophs are akin to phytoplankton on Earth, we specify $\mathcal{F}_C \sim 10$ μmol m^{-2} s^{-1} (Regaudie-De-Gioux & Duarte 2010; Ritchie et al. 2018); varying $\mathcal{F}_C$ by a factor of $\sim$2 (Nelson & Smith 1991; Siegel et al. 2002) exerts a minor influence on subsequent results via (6). Thus, by calculating the location where $\mathcal{F}(z) = \mathcal{F}_C$ is attained, one can duly determine the approximate location of the compensation depth.

In Figure 1, the maximal photon flux has been plotted as a function of the depth for Earth-analogs orbiting different stars. By making use of (6) and the threshold $\mathcal{F}_C$, we find that $\mathcal{Z}_{\rm CO}^{(M)} \approx 244$ m for a Sun-like star ($T = 5780$ K),[5] and $\mathcal{Z}_{\rm CO}^{(M)} \approx 16$ m for a late-type M-dwarf analogous to TRAPPIST-1 ($T = 2500$ K). These numbers are in reasonable agreement with the corresponding values of 185 m and 10 m calculated for Earth and Proxima b, respectively (Ritchie et al. 2018, Figure 7).

Next, we turn our attention to the case where time-averaged photon flux and biological attenuation are included. The ensuing results are depicted in Figure 2. For a Sun-like star, we estimate $\mathcal{Z}_{\rm CO}^{(R)} \approx 20$ m, whereas we find $\mathcal{Z}_{\rm CO}^{(R)} \approx 1$ m for a late-type M-dwarf with $T = 2500$ K. The former value is consistent with empirical estimates of $\sim$20–30 m for the compensation depth in multiple environments (Sverdrup et al. 1942; Siegel et al. 2002; Middelburg 2019). For both the maximal and realistic cases, we find that the compensation depth is reduced by more than an order of magnitude as one moves from Sun-like stars to the coolest M-dwarfs.

To undertake a similar calculation for anoxygenic photoautotrophs, two changes must be implemented. First, the longest wavelength suitable for photosynthesis must be extended to $\lambda_{\rm max} \approx 1000$ nm (Blankenship 2014, Chapter 1.2). Second, the photon flux at the compensation point is specified to be $\mathcal{F}_C \sim 1$ μmol m^{-2} s^{-1} based on the *Chlorobium* species extracted from lakes and fjords in Vestfold Hills, Antarctica (Burke & Burton 1988).[6] We can neglect the first factor without much loss of generality because water is strongly absorbing in the near-IR (Kou et al. 1993).

Upon utilizing this value of $\mathcal{F}_C$, we obtain $\mathcal{Z}_{\rm CO}^{(M)} \approx 500$ m and $\mathcal{Z}_{\rm CO}^{(M)} \approx 95$ m for a Sun-like star and late-type M-dwarf ($T = 2500$ K), respectively. In comparison, a similar analysis by Ritchie et al. (2018, Figure 8) yielded compensation depths of approximately 400 and 60 m for Earth and Proxima b. For the realistic scenario described previously, we find

[5] This result seems compatible with the detection of microalgae at depths of 285 m on Earth (Valiela 2015, Chapter 3.1).

[6] As per empirical data and theoretical constraints, $\mathcal{F}_C \sim 0.01$ μmol m^{-2} s^{-1} is compatible with anoxygenic photosynthesis (Raven et al. 2000; Manske et al. 2005), but the prior conservative limit is adopted for comparison against Ritchie et al. (2018).

$\mathcal{Z}_{\rm CO}^{(R)} \approx 40$ m and $\mathcal{Z}_{\rm CO}^{(R)} \approx 12$ m for the solar analog and the late-type M-dwarf.

Now, we turn our attention to gauging the critical depth ($\mathcal{Z}_{\rm CR}$), namely, the thickness of the aquatic layer where the vertically integrated photosynthetic growth rate exceeds the total loss rate due to respiration and other factors (Mann & Lazier 2006, Chapter 3). Thus, communities circulating in this layer are theoretically capable of survival and growth.[7] The estimation of $\mathcal{Z}_{\rm CR}$ is not straightforward because a number of divergent (albeit cognate) formulae exist: see Sarmiento & Gruber (2006, Equation (4.3.5)), Kirk (2011, Equation (11.1)), Mann & Lazier (2006, Equation (3.08)), and Middelburg (2019, Equation (2.27)). The expression provided in the last two references is equivalent to the classic result derived by Sverdrup (1953), and equals

$$\frac{1-\exp(-K\mathcal{Z}_{\rm CR})}{K\mathcal{Z}_{\rm CR}} = \frac{\Gamma_R}{\Gamma_P}, \tag{8}$$

where Γ_R and Γ_P denote the rates of respiration and maximal photosynthesis, respectively. This can be further simplified to yield $K\mathcal{Z}_{\rm CR} \approx \Gamma_P/\Gamma_R$ (Falkowski & Raven 2007, Equation (9.7)) because $K\mathcal{Z}_{\rm CR} \gg 1$ is valid.

As the above formula was obtained under the assumption of $K = $ const, it is necessary to recalculate $\mathcal{Z}_{\rm CR}$ for $K(\lambda)$. After implementing the same procedure (Mann & Lazier 2006, Chapter 3) we arrive at

$$\mathcal{Z}_{\rm CR} \approx \left(\frac{\Gamma_R}{\Gamma_P}\right)^{-1} \frac{\int_{\lambda_{\rm min}}^{\lambda_{\rm max}} [\mathcal{N}_0(\lambda)/K(\lambda)]d\lambda}{\int_{\lambda_{\rm min}}^{\lambda_{\rm max}} \mathcal{N}_0(\lambda)d\lambda}. \tag{9}$$

We specify $\Gamma_R/\Gamma_P \approx 3.36 \times 10^{-2}$ for putative biota (Sarmiento & Gruber 2006, Chapter 4.3) and adopt the parameters from the "R" case introduced earlier to facilitate comparison with prior studies that accounted for time-averaged photon flux and biological attenuation.

The resultant critical depth is plotted in Figure 3. The heuristic formula $\mathcal{Z}_{\rm CR} \approx 185\ {\rm m}\ \sqrt{T/T_\odot}$ displays excellent agreement (<5%) with the actual results. From (9), we obtain $\mathcal{Z}_{\rm CR}^{(R)} \approx 187$ m for the solar analog. This result compares favorably with the estimate of 170 ± 30 m for Earth's oceans (Siegel et al. 2002; Sarmiento & Gruber 2006) and 177 m for Lake Windermere, England (Kirk 2011, Chapter 11.1). For a late-type M-dwarf with $T = 2500$ K, we arrive at $\mathcal{Z}_{\rm CR}^{(R)} \approx 119$ m.

Thus, as evinced by Figure 3, the critical depth is relatively insensitive to the stellar temperature. This trend probably arises because the bulk of productivity occurs at shallow depths, where the rates of photosynthesis are much higher due to their near-linear dependence on $\mathcal{F}(z)$ (Mann & Lazier 2006; Sarmiento & Gruber 2006); as $\mathcal{Z}_{\rm CR}$ entails vertical integration, most of the contribution to net growth is from the upper layers. In principle, therefore, the extent of the zone wherein the integrated net growth of phytoplankton-like organisms is feasible remains roughly constant across Earth-analogs orbiting different stars. Moreover, as $\mathcal{Z}_{\rm CR}$ governs the initiation of phytoplankton blooms (Falkowski & Raven 2007), *ceteris paribus*, analogous phenomena may have a similar likelihood of occurrence on these worlds.

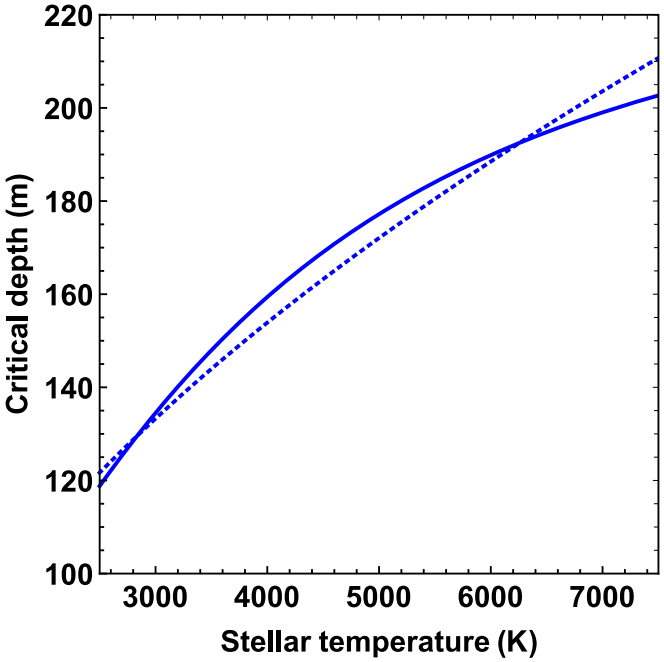

Figure 3. Critical depth (in m), the location at which the vertically integrated net growth rate becomes zero, as a function of stellar temperature (in K). Effects of time-averaged photon flux and aquatic biological attenuation are incorporated. The unbroken line corresponds to (9), whereas the dotted line depicts the power-law approximation given by $\mathcal{Z}_{\rm CR} \approx 185\ {\rm m}\ \sqrt{T/T_\odot}$.

3. Discussion and Conclusions

We estimated the compensation and critical depths for Earth-analogs around various stars. We determined that the former decreases by more than an order of magnitude as one moves from solar analogs to the smallest stars (i.e., late-type M-dwarfs); in contrast, the critical depth varies by merely ~40% across the same range.

Our work has several implications for life detection. Due to the lower compensation depth associated with late-type M-dwarfs, the rates of carbon fixation could be correspondingly lower, which is consistent with prior analyses of this subject (Wolstencroft & Raven 2002; Ritchie et al. 2018). Earth-analogs around these stars are expected to have lower likelihoods of building up oxygenated atmospheres because of diminished O_2 production rates (Lehmer et al. 2018; Lingam & Loeb 2019b). This would, in turn, give rise to "false negatives" insofar as life detection through atmospheric oxygen is concerned. Inability to accumulate atmospheric O_2 might also prove to be detrimental for the origin of complex multicellularity due to metabolic constraints (Catling et al. 2005; Lingam & Loeb 2019c).

Even if biologically oxygenated atmospheres are suppressed on M-dwarf exoplanets, the biomass density near the surface is nevertheless potentially comparable to that of Earth's oceans. In fact, due to the combined action of a slower rotation rate (induced by tidal locking) and stronger tidal forces, nutrient upwelling could increase on these worlds, thereby conceivably elevating the biomass density (Lingam & Loeb 2018; Olson et al. 2019). Hence, for sufficiently high coverage and density of oxygenic photoautotrophs, the photosynthetic red edge (PRE) may facilitate the detection of life. In the absence of

[7] Although the critical depth hypothesis constitutes a vital concept in biological oceanography, some of its underlying postulates and consequent predictions have been challenged (Behrenfeld 2010).

cloud cover and 50% surface coverage by oceanic cyanobacteria, O'Malley-James & Kaltenegger (2019, Table 1) estimated that the reflected flux would increase by 10% at the PRE. Hence, for such tidally locked planets, the reflected flux at the PRE ought to vary between 0% and ∼10% over an orbital period, thus possibly rendering this biofeature amenable to detection.

The expression of a surface signature from anoxygenic photosynthesis or non-photosynthetic organisms may have occurred on the Archean Earth prior to the evolution of oxygenic photosynthesis and detectable levels of its atmospheric signature (Schwieterman et al. 2018). The PRE, however, is widely considered unlikely to have been detectable prior to the emergence of vegetation on land (Lyons et al. 2014). Based on modeling by O'Malley-James & Kaltenegger (2019), our work suggests that the PRE might be discernible even in the absence of a detectable O_2 biosignature.

There are several caveats that merit reiteration. Perhaps most importantly, we assumed that the functional traits of putative photoautotrophs were akin to eukaryotic phytoplankton. The spectral diversity and flexibility of cyanobacteria analogs, especially their capacity to utilize chlorophylls d and f at far-red and near-IR wavelengths (Nürnberg et al. 2018; Schwieterman et al. 2018), might render them increasingly important for cool stars. As the predominant cyanobacteria species can grow at photon fluxes that are ∼10 times smaller than the compensation flux considered herein (Canfield et al. 2005, Chapter 3.2.1) our results must be revised upward by a factor of $\lesssim$10 in accordance with Figures 1 and 2.

We also neglected deviations from the blackbody spectrum and the deleterious effects of stellar flares. However, with regards to the latter, a combination of screening compounds, strong absorption by water at ultraviolet wavelengths, and physiological adaptations (e.g., DNA repair) may collectively ensure that organisms are protected several meters underwater (Cleaves & Miller 1998; Lingam & Loeb 2019c). Last, but not least, we have not addressed the crucial issue of nutrient limitation in this Letter. Ocean planets, for instance, have been predicted to possess limited biospheres due to low rates of phosphate supply from weathering (Wordsworth & Pierrehumbert 2013; Lingam & Loeb 2019d).

Despite these caveats, our model retains sufficient complexity (without sacrificing simplicity), consequently enabling us to make concrete and testable predictions. In particular, if future spectroscopic and photometric observations of M-dwarf exoplanets detect no evidence of biotic O_2 in the atmosphere and find evidence for the PRE, this would lend credence to the notion that these worlds might host an unusual combination of fairly dense but shallow aquatic biospheres.

This research was supported in part by the Breakthrough Prize Foundation, Harvard University's Faculty of Arts and Sciences, and the Institute for Theory and Computation (ITC) at Harvard University.

ORCID iDs

Manasvi Lingam https://orcid.org/0000-0002-2685-9417
Abraham Loeb https://orcid.org/0000-0003-4330-287X

References

Barnes, R. 2017, CeMDA, 129, 509
Behrenfeld, M. J. 2010, Ecology, 91, 977
Blankenship, R. E. 2014, Molecular Mechanisms of Photosynthesis (2nd ed.; New York: Wiley-Blackwell)
Burke, C. M., & Burton, H. R. 1988, HyBio, 165, 13
Canfield, D., Kristensen, E., & Thamdrup, B. 2005, Aquatic Geomicrobiology, Advances in Marine Biology No. 48 (Amsterdam: Elsevier)
Catling, D. C., Glein, C. R., Zahnle, K. J., & McKay, C. P. 2005, AsBio, 5, 415
Chen, M., & Blankenship, R. E. 2011, Trends Plant Sci., 16, 427
Cleaves, H. J., & Miller, S. L. 1998, PNAS, 95, 7260
Falkowski, P. G., & Raven, J. A. 2007, Aquatic Photosynthesis (2nd ed.; Princeton, NJ: Princeton Univ. Press)
Field, C. B., Behrenfeld, M. J., Randerson, J. T., & Falkowski, P. 1998, Sci, 281, 237
Grimm, S. L., Demory, B.-O., Gillon, M., et al. 2018, A&A, 613, A68
Jacob, D. J. 1999, Introduction to Atmospheric Chemistry (Princeton, NJ: Princeton Univ. Press)
Kaltenegger, L. 2019, BAAS, 51, 502.05
Kasting, J. F., Whitmire, D. P., & Reynolds, R. T. 1993, Icar, 101, 108
Kiang, N. Y., Segura, A., Tinetti, G., et al. 2007, AsBio, 7, 252
Kirk, J. T. O. 2011, Light and Photosynthesis in Aquatic Ecosystems (3rd ed.; Cambridge: Cambridge Univ. Press)
Knoll, A. H. 2015, Life on a Young Planet: The First Three Billion Years of Evolution on Earth (Princeton, NJ: Princeton Univ. Press)
Kou, L., Labrie, D., & Chylek, P. 1993, ApOpt, 32, 3531
Lee, Z., Weidemann, A., Kindle, J., et al. 2007, JGRC, 112, C03009
Lehmer, O. R., Catling, D. C., Parenteau, M. N., & Hoehler, T. M. 2018, ApJ, 859, 171
Lingam, M., & Loeb, A. 2018, AsBio, 18, 967
Lingam, M., & Loeb, A. 2019a, ApJ, 883, 143
Lingam, M., & Loeb, A. 2019b, MNRAS, 485, 5924
Lingam, M., & Loeb, A. 2019c, RvMP, 91, 021002
Lingam, M., & Loeb, A. 2019d, AJ, 157, 25
Lyons, T. W., Reinhard, C. T., & Planavsky, N. J. 2014, Natur, 506, 307
Mann, K. H., & Lazier, J. R. N. 2006, Dynamics of Marine Ecosystems: Biological-Physical Interactions in the Oceans (3rd ed.; Oxford: Blackwell)
Manske, A. K., Glaeser, J., Kuypers, M. M. M., & Overmann, J. 2005, Appl. Environ. Microbiol., 71, 8049
Middelburg, J. J. 2019, Marine Carbon Biogeochemistry: A Primer for Earth System Scientists, SpringerBriefs in Earth System Sciences (Berlin: Springer)
Nelson, D. M., & Smith, W. O. 1991, LimOc, 36, 1650
Nürnberg, D. J., Morton, J., Santabarbara, S., et al. 2018, Sci, 360, 1210
Olson, S. L., Jansen, M., & Abbot, D. S. 2019, ApJ, submitted (arXiv:1909.02928)
O'Malley-James, J. T., & Kaltenegger, L. 2019, ApJL, 879, L20
Pope, R. M., & Fry, E. S. 1997, ApOpt, 36, 8710
Raven, J. A. 2009, Aquat. Microb. Ecol., 56, 177
Raven, J. A., Kübler, J. E., & Beardall, J. 2000, J. Mar. Biol. Assoc. UK, 80, 1
Regaudie-De-Gioux, A., & Duarte, C. M. 2010, GBioC, 24, GB4013
Ritchie, R. J., Larkum, A. W. D., & Ribas, I. 2018, IJAsB, 17, 147
Sarmiento, J. L., & Gruber, N. 2006, Ocean Biogeochemical Dynamics (Princeton, NJ: Princeton Univ. Press)
Schwieterman, E. W., Kiang, N. Y., Parenteau, M. N., et al. 2018, AsBio, 18, 663
Siegel, D. A., Doney, S. C., & Yoder, J. A. 2002, Sci, 296, 730
Sverdrup, H. U. 1953, J. Cons. Perm. Int. Explor. Mer, 18, 287
Sverdrup, H. U., Johnson, M. W., & Fleming, R. H. 1942, The Oceans: Their Physics, Chemistry, and General Biology (Englewood Cliffs, NJ: Prentice-Hall)
Tian, F., & Ida, S. 2015, NatGe, 8, 177
Unterborn, C. T., Hinkel, N. R., & Desch, S. J. 2018, RNAAS, 2, 116
Valiela, I. 2015, Marine Ecological Processes (3rd ed.; Berlin: Springer)
Ward, L. M., Rasmussen, B., & Fischer, W. W. 2019, JGRG, 124, 211
Wolstencroft, R. D., & Raven, J. A. 2002, Icar, 157, 535
Wordsworth, R. D., & Pierrehumbert, R. T. 2013, ApJ, 778, 154
Yang, J., Cowan, N. B., & Abbot, D. S. 2013, ApJL, 771, L45
Zain, P. S., de Elía, G. C., Ronco, M. P., & Guilera, O. M. 2018, A&A, 609, A76